Research Journal of Medical Sciences 10 (4): 374-393, 2016
ISSN: 1815-9346

Cardiac Diffusion-Weighted Imaging: From the Physics to Clinical Applications

[1]Ali Nahardani, [1]Fariborz Faeghi and [2]Hasan Hashemi
[1]Department of Radiology Technology, School of Allied Medical Sciences,
Shahid Beheshti University of Medical Sciences, Tehran, Iran
[2]Department of Radiology, Tehran University of Medical Sciences, Tehran Iran

Abstract: The human cardiovascular system is a complex architecture consisting of an uncountable number of muscular fibers. This architecture is orderly arranged. Most of the cardiovascular diseases affect the microstructural normal histology and thereby its regularity (e.g., Hypertrophic cardiomyopathy, myocarditis, etc.). Diffusion-weighted imaging is a neuroradiological method to image the early neural histopathological changes in cerebrovascular accidents non-invasively. It can be employed on the other highly organized tissues like the myocardium. Cardiac Diffusion Tensor Imaging (DTI) is a novel and promising method for investigating the myocardial fibrous structure non-invasively. DTI measures the magnitude of diffusivity and provides the information regarding the myocardial fibers' orientations in space. This study reviews the precise definition of the diffusion phenomenon from biological and physical points of view and then explains the cardiac diffusion-weighted and diffusion tensor imaging methods. It also introduces the practical maps and indices to interpret the myocardial microstructures correctly and then reviews the cardiac diffusion imaging's clinical applications briefly. Finally, a concise discussion of the cardiac diffusion tensor imaging's drawbacks and limitations is held to pave the road for other researchers and investigators.

Key words: Magnetic resonance imaging, diffusion tensor imaging, diffusion weighted MRI, cardiac imaging, echo-planar imaging

INTRODUCTION

Magnetic Resonance Imaging (MRI) is a critical imaging tool in cardiovascular sciences. In contrast with the other imaging modalities, MRI benefits from a variety of weighting mechanisms (T1, T2, etc.). Diffusion Weighted Imaging (DWI) is one of the most recently developed methods in MRI. It measures the water molecules' average diffusivity in a voxel. DWI provides Diffusion-Weighted (DW) contrast. Many pathologic conditions change the tissues' microstructural compositions and alter their harmonic cell's arrays. The histological alteration results in diffusion pattern changes. For instance, the water molecules' diffusivity becomes restricted in the case of cellular swelling. As a result, diffusion weighted imaging is a potentially powerful probe to roughly characterize the histopathology if measured precisely. Since, the introduction of the DWI in 1985 (Le Bihan *et al*., 1986) novel modifications have been made to extend our ability to study the tissues' microstructures. One of these developments is the Diffusion Tensor Imaging (DTI). DTI provides reliable information about the tissues' microstructural diffusion patterns and orientations. In the regions with fiber crossing, kissing and curving, DTI shows a limited potential to image the fibers' orientations accurately; thus, more sophisticated techniques like Q-Ball imaging are introduced (Basser *et al*., 1994; Conturo *et al*., 1999; Mori *et al*., 1999, Basser *et al*., 2000).

Cardiac MRI is facing a revolution, the revolution of diffusion imaging. Cardiac Diffusion Tensor Imaging (cDTI) has emerged recently and is under investigations. cDTI gives useful information about the myocardial fibers' spatial orientations and their correlations with the different electrocardiographic systolic and diastolic phases (McGill *et al*., 2016). It allows clinicians to diagnose recent Myocardial Infarctions (MIs) and differentiate it from chronic ones in patients with severe renal dysfunctions, who are contraindicated to gadolinium injection (Laissy *et al*., 2013). It is a great imaging modality to characterize different pericardial lesions and helps to its differential diagnosis in a great extent (Raja *et al*., 2011; Ozmen *et al*., 2015).

Cardiac Diffusion Weighted Imaging (cDWI) is an almost new technique that seems to have a great potential to change the practice of cardiac imaging. In this study, a

Corresponding Author: Ali Nahardani, Department of Radiology Technology, School of Allied Medical Sciences, Shahid Beheshti University of Medical Sciences, Tajtish Squar, Postal Code 1971653313, Tehran, Iran

thorough review of the diffusion phenomenon, diffusion-weighted imaging, diffusion tensor imaging, cardiac diffusion MRI methodologies, practical DTI interpretative indices and cDTI's clinical applications are provided. Finally, a comprehensive discussion about the cardiac diffusion imaging drawbacks and limitations is opened up.

MATERIALS AND METHODS

In our research, we queried the keywords of "Diffusion Weighted Imaging, Cardiac MRI, Cardiac Diffusion Imaging, Cardiac Diffusion tensor Imaging, Cardiac Tractography, Cardiac Q-ball Imaging" in all the PubMed/ScienceDirect/ISI indexed journals and abstracted our finding as.

Diffusion: from Biology to mathematical modeling: In 1827, a Scottish botanist called Robert Brown observed the random motion of suspended particles in a type of fluid for the first time. He was investigating the tiny pollen grains of the *Clarkia pulchella* species under the microscope and incredibly observed that those pollen grains were moving randomly under the microscope. He was intrigued by those movements but was not able to determine the mechanisms underlying it. So, he examined alive and dead pollen grains from other species to investigate its occurrence in other ones. Finally, he observed the same random movements in all of his samples. Now a days, we know that the motion that Brown observed is not arising from the "essence of life" as he proved it but is due to the bombardment of pollen grains by the gas or liquid molecules at different thermal energy states. The random molecular motion is sometimes called the Brownian motion or simply as diffusion. The probe of diffusion is the main goal of DTI. Diffusion is an essential physical process in the normal functioning living tissues; For instance, the active potential. The active potential is the transport of sodium and potassium ions through the cellular membrane. The active potential is founded on the diffusion and is the primary way of muscular contraction transfer along the myocardial fibers. Studying diffusion provides deep insights into the both cell physiology and cell structure (Gillard *et al*., 2005; Hall and Guyton 2011).

Diffusion is a phenomenon at the molecular level. It is described by the transfers of molecules (e.g., water molecules) from one location to the others during a period of time. It is random and can occur in every direction. The laws of diffusion were described by Fick (1855) for the first time. The Fick's first law of diffusion states that the diffusion flux density is linearly proportional to the concentration gradients (Eq. 1) and his second law of diffusion predicts how diffusion makes the molecular concentration change over time (Eq. 2):

$$J = -D\frac{\partial \varphi}{\partial x} \quad (1)$$

$$\frac{\partial \varphi}{\partial t} = D\frac{\partial^2 \varphi}{\partial x^2} \quad (2)$$

Where:

J = The "diffusion flux density" (mol m^{-2} s)
D = The "diffusion coefficient" (m^2 s^{-1})
φ = The "molecular concentration" (mol m^{-2})
x = The "length" (m)
t = The "time" (sec)

Based on the Fick's first law of diffusion, the constant of proportionality is equal to the diffusion coefficient. Therefore, the diffusion coefficient can be estimated by measuring the sample's concentration over time (Fick, 1855; Gillard *et al*., 2005).

In 1905, Albert Einstein introduced a formula in the three-dimensional space that explains the mean molecular displacement as a function of time. Einstein stated that the molecular displacement was directly proportional to a constant that changes in every type of material. For instance, this constant is changed by the material's viscosity. He named this constant "diffusivity". Based on the Einstein's equation of diffusion (Eq. 3), Diffusivity (D) is proportional to the mean squared molecular displacement (r^2) divided by the number of measuring dimensions (n) and the measring time (t). The pure water's diffusion coefficient is roughly 2.0×10^{-3} m^2 s^{-1} at 20°C and increases at higher temperatures (Einstein, 1956; Gillard *et al*., 2005; Alexander *et al*., 2007):

$$D = \frac{\left(r^2\right)}{2nt} \quad (3)$$

Equation 3 scale is metric. In the absence of boundaries, the free water molecular displacement is described by a univariate Gaussian probability density/distribution function as expressed as below (Eq. 4) (Alexander *et al*., 2007):

$$P(\Delta r, \Delta t) = \frac{1}{\sqrt{2nDt^3}} e\left(\frac{-r^2}{4Dt}\right) \quad (4)$$

Based on Eq. 4, the water molecules' concentration lowers in space by the passage of time (t). The distance moved by each molecule increases over time

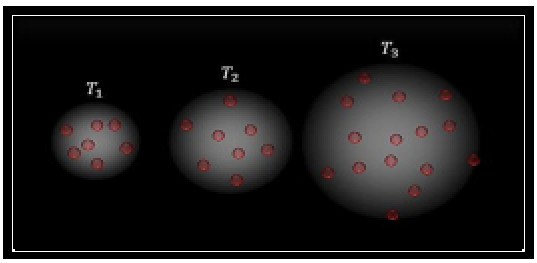

Fig. 1: Represents two-dimensional water molecules' displacement probability as a function of time. Initially, The molecular concentration is compact (T_1) but its concentration decreases over tome (T_2 and T_3). The molecular average displacement is higher in T_3 than in T_1. This illustration is a graphical explanation of the Einstein's equation of diffusion

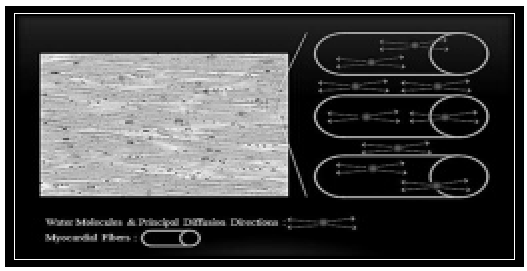

Fig. 2: Represents the principal diffusion direction along the myocardial fibers schematically. The water diffusion is relatively unhindered in the directions parallel to the fiber orientations in a highly organized tissue like myocardium. In contrast, it is highly restricted in the perpendicular directions to the myocardial fibers. Therefore, the diffusion is assumed anisotropic in the myocardial tissue

(Fig. 1). Surprisingly, the Gaussian diffusion probability density/distribution function is not true for most of the living tissues' microstructures, especially in the regions with fiber crossing, kissing and curving. (Tuch *et al*., 2002; Berman *et al*., 2013).

In biological tissues, the water molecule's diffusion occurs inside, outside and through cellular membranes. It occurs even inside of an organelle but its magnitude is not comparable with the extracellular space diffusion. Water Brownian motion is primarily due to the random thermal and molecular kinetic energies fluctuations. The different kinetic energy levels lead to the process of diffusion. The diffusion does not occur freely in living tissues and is further modulated by aqua-phobic cellular and sub-cellular membranes. Cellular membranes are hydrophobic and hinder the water molecules' diffusion perpendicular to them, causing the molecules to displace in a more tortuous path along them. Restriction always results in a decrease in the apparent diffusion coefficient. Both the cytotoxic edema and hypercellularity may decrease the water molecular diffusivity. Conversely, necrosis decreases the tortuosity and increases the apparent diffusion coefficients (Le Bihan, 1995; Moritani *et al*., 2005; Alexander *et al*., 2007). The water diffusion is relatively unhindered in the directions parallel to the fiber orientations in an organized tissue. In contrast, it is highly restricted in the perpendicular directions to them. Thus, the diffusion is anisotropic in highly organized tissues like myocardium. Anisotropic diffusion means that the mean molecular displacement is not equal in every direction and is lower or higher in at least one dimension (Fig. 2) (Chenevert *et al*., 1990; Moseley *et al*., 1990; Gillard *et al*., 2005).

The univariate Gaussian probability density distribution model is usually used to measure the tissues' diffusivities unidimensionally (in one direction), but it is not a good model to characterize it in a multidimensional space. For this reason, Basser et al introduced a diffusion tensor model to describe the anisotropic diffusion behavior. In their model, the water diffusion was described by a multivariate normal distribution function (Basser *et al*., 1994a, b; Alexander *et al*., 2007):

$$P(\Delta r,\Delta t)=\frac{1}{\sqrt{(4\pi\Delta t)^3|D|}}e\left(\frac{-\Delta\bar{r}^2D^{-1}\Delta\bar{r}}{4\Delta t}\right) \quad (5)$$

Where $|D|$ is a 3×3 covariance diffusion tensor (Basser *et al*., 1994a, b; Alexander *et al*., 2007):

$$|D|=\begin{bmatrix}D_{xx} & D_{xy} & D_{xz}\\ D_{yx} & D_{yy} & D_{yz}\\ D_{zx} & D_{zy} & D_{zz}\end{bmatrix} \quad (6)$$

The diffusion tensor matrix is a symmetric square matrix with 9 elements. The diffusion tensor matrix describes the diffusion displacements covariance (normalized by the diffusion time) in three-dimensional space. The diagonal elements (D_{xx}, D_{yy}, D_{zz}) correspond to the diffusivities along the three Cartesian orthogonal axes (x,y,z). It is essential to realize that the diffusion tensor's off-diagonal elements do not represent diffusivities through themselves. For example, the element D_{xy} is not

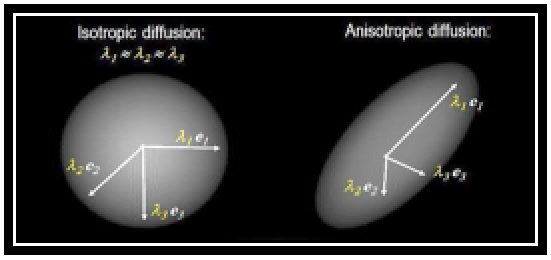

Fig. 3: Represents the isotopic (A) versus anisotropic (B) diffusion models. Diffusion is considered to be isotropic when the eigenvalues are nearly equal (e.g., $\lambda_1 \sim \lambda_2 \sim \lambda_3$). Conversely, the diffusion tensor is called to be anisotropic when the eigenvalues are significantly different in magnitude ($\lambda_1 > \lambda_2 > \lambda_3$)

the diffusivity in the xy direction. The off-diagonal elements reflect the correlation between two orthogonal diffusivities. For obtaining tissues' diffusion information (such as the magnitude and the diffusion direction), a mathematical operation called diagonalization should be performed on the diffusion tensor. Diagonalization changes all the diagonal and off-diagonal diffusivities and provides new quantities called eigenvectors (ε_1, ε_2, ε_3) and eigenvalues (λ_1, λ_2, λ_3). Eigenvectors represent the principal diffusion directions relative to the standard Cartesian orthogonal axes and Eigenvalues describe the apparent diffusivities along those directions. Diffusion tensor might be visualized by an ellipsoid. The ellipsoid's size and orientation are determined by the eigenvalues and eigenvectors. Diffusion is considered to be isotropic when all the eigenvalues are nearly equal ($\lambda_1 \sim \lambda_2 \sim \lambda_3$). Conversely, the diffusion is called to be anisotropic when the eigenvalues are significantly different with each other ($\lambda_1 > \lambda_2 > \lambda_3$) (Fig. 3). Eigenvalues may be affected by any histopathological changes in the local tissues' microstructures. Therefore, the diffusion tensor is a sensitive probe for characterizing both the normal and diseased tissues from each other (Gillard *et al*., 2005; Alexander *et al*., 2007).

In most of the living tissues, the diffusion model is anisotropic rather than isotropic (especially in the myocardium) and there is more than one fiber orientation in each voxel (Gillard *et al*., 2005; Alexander *et al*., 2007). Those regions usually have a pancake-shaped ellipsoid and contain crossing, kissing or curving fibers. In those regions, none of the uni-or multi-variate Gaussian probability density/distribution models cannot characterize the diffusion magnitudes and orientations correctly. Consequently, there is a need for a more complex model to characterize diffusion. In the recent years, directly measurement of diffusion anisotropy has become quite popular since it overcomes the Gaussian probability density/distribution models' limitations and can map voxels' fibers' orientations precisely (Tuch *et al*., 2002; Mori and Tournier, 2013).

Diffusion imaging

MRI basics: Magnetic Resonance Imaging (MRI) is a medical imaging modality in medicine. MRI's scanner is a very large magnet, using radiofrequency waves and powerful magnetic field gradients to image different parts of the body. There are different types of chemical elements in the human body. The most abundant element is hydrogen or more precisely Protium. Protium consists of a proton and electron. Its atomic number is one and its nucleus is electrically positive. The Protium nucleus has a rotation around its main longitudinal axis thus, based on the Faraday's law of induction, it produces a tiny magnetic field around itself. In fact, all the Protium nuclei are tiny magnets. The Protium nuclei's distribution and alignment are random out of an external strong magnetic field. In the existence of an external magnetic field, the Protium nuclei experience two different types of motion, the spin alignment and precessional rotation. When the human body is placed inside the MRI's scanner, the Protium nuclei redistribute themselves to become aligned with the MRI scanner's magnetic field lines. They become either parallel or anti-parallel to it, i.e., they realign towards either the patient's head or feet, with approximately 50% going either way and effectively canceling each other out. About 0.0001-0.0002% of Protium nuclei remain unmatched and would not be canceled out; consequently, they create a Net Magnetization Vector (NMV) in the human body. When the body is positioned in the MRI's scanner, the Protium nuclei experience a precessional rotation around the main magnetic field lines too. The rotation has a frequency and is called the Larmor frequency. The Protium nuclei's Larmor frequency is 42.58 MHz per tesla.

While the human body is inside the MRI's scanner, a set of specific Radio Frequency (RF) pulse (B_1) with the Protium nuclei's Larmor frequency is applied to the interested body part. As a result, the NMV absorbs the RF pulse energy and flips from its original alignment along the z-axis. The angulation is called "Flip Angle" or (FA). When the RF pulse is ceased, the net magnetization vector returns to its original equilibrium energy state and induces some signals into the RF coil. The RF coil sends the signal to a computer and a mathematical operation

called Inverse Fourier Transformation (IFT) is performed on the raw signals. IFT converts the original signal and data series (k-space) into an interpretable image for clinicians. It is important to note that, a series of the gradient magnets switch on and off during RF pulse transmission and create the magnetic field gradients. The magnetic field gradients change the main magnetic field at a predefined slope and allow sectional images to be acquired (Hashemi and Lisanti, 2010).

The induced MRI signals decay over time. The signal's deterioration is usually analyzed in terms of two relaxation phenomenon, the longitudinal relaxation (T1) and the transverse relaxation (T2). Both the longitudinal and transverse relaxation phenomena have their own time constants, T1 and T2 relaxation time, respectively. Longitudinal relaxation is responsible for the induced signal's amplitude and the other one, T2 is responsible for the signal's broadening and decay over time (Lee *et al*., 2005).

T1 relaxation time: The T1 relaxation phenomenon is the NMV's longitudinal component's (M_z) return to its original thermal equilibrium value ($M_{(z, e, q)}$) post-excitation. If the NMV was flipped into the transverse plane, the T1 relaxation phenomenon could simply be defined by the equation below as a function of time (t):

$$M_z(t) = M_{(z,e,q)}\left(1 - e^{\frac{-t}{T1}}\right) \quad (7)$$

It can be inferred that the T1 relaxation time is the required time for M_z to recover to the 63% of its primary original value after the 90° RF pulse excitation and cease (Lee *et al*., 2005).

T2 relaxation time: In an external magnetic field, the Protium nuclei experience the Larmor precession too. The Larmor precession is the main source of spin incoherence in a small tissue volume. When the hydrogen nuclei are exposed to an external RF pulse, they overcome their incoherence and become rephased with each other; thus, creating a magnetization along the transverse (xy) plane. The transverse relaxation phenomenon can be expressed as the decay of the nuclei maximum coherence after the RF pulse cease. When the RF pulse is ceased, the hydrogen nuclei gain their initial incoherence again and the transverse disappears steadily. The T2 relaxation phenomen on can be defined as a function of time (t) (Lee, *et al*., 2005):

$$M_{xy}(t) = M_{xy}(0)e^{\frac{-t}{T2}} \quad (8)$$

It can be inferred that the T2 relaxation time is the required time for transverse magnetization (M_{xy}) to drop to 37% of its initial original magnitude after the RF excitation pulse exposure (Lee *et al*., 2005). The Nuclear Magnetic Resonance (NMR) concept was introduced by Isidor Isaac (Rabi *et al*., 1938). In 1946 Felix Bloch expanded the NMR techniques and defined some equations that were used to calculate the nuclear magnetization M = (M_x, M_y,M_z) as a function of time and T1/T2 relaxation phenomena (Bloch, 1946). Up to the year of 1956, T1 and T2 relaxations were two golden physical phenomena to analyze and characterize the compositions of complex materials but a great discovery emerged in 1956 that led to the introduction of the diffusion-weighted imaging. In that year, a scientist called Torrey showed that how the molecular diffusion would change the NMR signal. Torrey modified Bloch's original description of nuclear magnetization and added a diffusion term to it (Torrey, 1956; Rohmer and Gullberg, 2006).

Diffusion-weighted imaging: Diffusion-weighted imaging is an MRI technique that came into existence in the mid-1980s (Le Bihan *et al*., 1986). It allows clinicians and scientists to map the molecular diffusion *in vivo* and non-invasively. In living systems, molecular diffusion is not free and is anisotropic. Different tissues have different diffusion coefficients. Diffusion-weighted imaging is the method that produces MR images with the diffusion contrast *in vivo*, i.e., its contrast is reconstructed based on the tissues' diffusivities (Posse *et al*., 1993).

Physics: There are numerous methods to image diffusion phenomenon in cardiac MRI. The most common *ex-vivo* imaging method is the Pulsed Gradient Spin Echo (PGSE). It is sometimes called the Stejskal-Tanner method. The Stejskal-Tanner method can be implemented on every readout gradient scheme. Diffusion-weighted imaging should be very fast in the cardiothoracic imaging; thus, the Stejskal-Tanner method is usually modulated on the Echo Planar Imaging (EPI) pulse sequence (Fig. 4). The PGSE-EPI is fast, insensitive to small motion, readily available on most clinical MRI scanners and its image quality is acceptable (Mansfield, 1984; Turner *et al*., 1990).

The simplest configuration of the PGSE-EPI pulse sequence uses a pair of large gradient pulses placed on both sides of the 180° refocusing pulse with the same

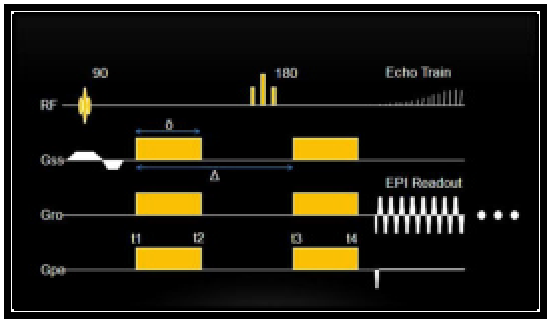

Fig. 4: Schematic representations of the PGSE-EPI sequence which was introduced by Stejskal and Tanner for the first time. The diffusion-encoding gradients are applied in two matched pulses. The gradient pulses duration is δ and their temporal separation is Δ

polarity and strength. The first gradient pulse dephases the magnetizations across the sample and the second one rephases them into their initials. For the stationary nuclei, the phase shifts (induced by both gradient pulses) will completely cancel each other out and the net magnetization will become maximally coherent. Consequently, the NMR signal will be so strong in the case of diffusion restriction. However, in the case of free diffusion, the diffusing nuclei will gain extra phase shifts in comparison with their initial phases and the diffusion gradient's second lobe cannot rephase the nuclei completely. As a result, the regions with low or restricted diffusivities will appear bright on the diffusion-weighted images and the regions with high diffusivities appear dark (Gillard *et al*., 2005).

The NMR signal's attenuation depends on various factors, depending on the implemented pulse sequence and interested tissues. The phase shifts' extent depends on the diffusion gradient pulses' amplitude, duration and the time interval between them as well as the water molecules' diffusivity. For the simple isotropic Gaussian diffusion, the signal attenuation for the Stejskal and Tanner method can be described by Eq. 9 (Stejskal and Tanner, 1965; Hashemi and Lisanti, 2010; Mori and Tournier, 2013):

$$S = S_0 e^{-bD} \quad (9)$$

Where:
S = The DW signal
S_0 = The non-diffusion weighted signal
D = The apparent diffusion coefficient
b = Stands for the b-value

the b-value is adjusted by the MRI technologist. It is the parameter that determines how much an image will become diffusion-weighted. In the PGSE method, b-value is described by Eq. 10 (Stejskal and Tanner, 1965; Mori and Tournier, 2013):

$$b = (\gamma G \delta)^2 \left(\Delta - \frac{\delta}{3} \right) \quad (10)$$

Where:
γ = The gyromagnetic coefficient
G = The gradient strength
δ = The applied gradient pulse's duration
Δ = The first and second diffusion gradient pulses' time interval

The b-factor can be altered by either changing the Gradient strength (G), the temporal separation of the gradients (Δ) or their duration (δ). High b-values increase the images' diffusion-weighting and diffusion contrast. It is analogous to the echo time in T2-weighted imaging (Stejskal and Tanner, 1965; Mori and Tournier, 2013). Andrew D. Scott showed that the optimum b-value for cardiovascular applications was 750 sn mm^{-2} (Basser *et al*., 1994a, b; Basser and Jones, 2002).

The simplest form of the Stejskal-Tanner method can be divided into four time-points as represented in Fig. 4 t_1-t_4. Mathematically, when a diffusion gradient pulse with the strength of G and the duration of δ is applied on a sample tissue, the Protium nuclei's phases change not only as a function of their spatial location but also time (because diffusion is a temporally dynamic phenomenon):

$$\varphi(x,t) = e^{\int i\gamma G_t t x} \quad (11)$$

Where:
φ = The resultant phase shift in the location of x
γ = The gyromagnetic ratio
G = The diffusion gradient pulse's strength
δ = The diffusion gradient pulse's duration
t = Stands for time

The diffusion phenomenon is assumed to follow the Gaussian Probability/distribution Density Function (PDF). Tissues have different diffusivities and owning different PDFs. The isotropic materials have wider PDFs than the anisotropic ones. An infinite fully restricted diffusion could be represented by a PDF with zero width. It is expected that the tissues' PDFs influence the overall NMR signal. WiderPDFs mean more molecular displacement and the more phase shifts during the diffusion gradient pulses applications. Therefore, the predicted signal could be calculated in the absence of the relaxation phenomena and just based on the nuclear magnetization coherence as follow:

$$S = \sum_{x} P(\Delta x, \Delta t)\varphi(x,t) \quad (12)$$

Equation 12 is classified discretely but the diffusion phenomenon and phase dispersions are continuous in the real world. In this case, the continuous form of the Eq. 12 could be rewritten as:

$$S = \frac{1}{\sqrt{(2nD\Delta t)^3}} \int_x e\left(\frac{-\Delta x^2}{4D\Delta t}\right) e^{\int i\gamma G(t)} dx \quad (13)$$

If n = 1, The Eq. 13's integration would result into:

$$S = S_o e - D\gamma^2 \int_{t1}^{t4} \left(\int_o^t G(t')dt'\right)^2 dt \quad (14)$$

Or

$$\ln\left(\frac{S}{S^o}\right) = -D\gamma^2 \int_{t1}^{t4} \left(\int_o^t G(t')dt'\right)^2 dt \quad (15)$$

There is a double integration over time in the Eq. 15. The term calculates the diffusion gradient pulse's area under the curve from t_1-t_2. The integration term $\int_{t1}^{t4} A^2 dt$ of integrates the term $A = \int_0^t G(t')dt'$ over the time course of t_1-t_2, t_2-t_3 and t_3-t_4 (Fig. 3). Therefore:

$$\ln\left(\frac{S}{S_o}\right) = -D\gamma^2 \left(\begin{array}{l} \int_{t1}^{t2} (Gt)^2 dt + \int_{t2}^{t3} (G\delta)^2 dt + \\ \int_{t1}^{t2} (G\delta - G(t - t_3))^2 dt \end{array}\right) \quad (16)$$

By the substitution of the different integration time points by the familiar timing symbols (δ and Δ) the Eq. 16 can be resolved and results into the Eq. 17:

$$\ln\left(\frac{S}{S_o}\right) = -D\gamma^2 G^2 \delta^2 \left(\Delta - \frac{\delta}{3}\right) \quad (17)$$

Which is the well-known PGSE diffusion-weighted imaging signal equation or Eq. 9. In conventional diffusion-weighted imaging, diffusion-encoding gradients are applied just in one direction to measure the diffusivity but it is problematic. In anisotropic tissues, diffusivity measurement in different diffusion directions results in different values. Diffusivity is called to be rotationally and spatially variant. One solution to overcome this problem is to measure diffusivities in a numerous number of directions and averaging the results; i.e., minimally in three orthogonal directions (Stejskal, 1965; Stejskal and Tanner, 1965; Le Bihan *et al*., 1986; Basser and Jones, 2002; Gillard *et al*., 2005).

Diffusion tensor imaging

Physics: Diffusion Tensor Imaging (DTI) provides wealthy information on the molecular diffusion patterns and principal directions in the living tissues. A variety of parameters and maps can be estimated from DTI, such as the Apparent Diffusion Coefficients (ADC) diffusion anisotropy (FA, RA, VR, etc.,) and the principal diffusion direction maps. These parameters indicate the tissues' microstructures. Presently, the clinical DTI's applications are primarily focused on the central nervous system (Filippi *et al*., 2001; Gupta *et al*., 2005; Kastrup *et al*., 2005; Lee *et al*., 2005; Malik *et al*., 2006; Romano *et al*., 2006; Trivedi *et al*., 2006 a, b; Utsunomiya *et al*., 2006; Gupta *et al*., 2006; Krageloh-Mann and Horber, 2007; Gupta *et al*., 2008; Wang *et al*., 2015) but its applications in the breast, prostate, kidney and cardiac imaging fields are under heavy investigations (Manenti, *et al*., 2007; Zhang *et al*., 2008; Eyal *et al*., 2012; Mekkaoui *et al*., 2015).

In contrast with the diffusion-weighted imaging, the simplest form of DTI acquires the diffusion data in at least six different directions (x, y, z, xy, xz and yz). The b-values are constant. During the acquisition, seven images are acquired from the same slice. Six of them have a b > 0 and one with a b = 0. The image intensities at each diffusion direction are attenuated depending on the diffusion gradient's strength and relative direction to the local fiber microstructures' orientations. Greater diffusivities result in more signal attenuation (Gillard *et al*., 2005; Moritani *et al*., 2005; Hagmann *et al*., 2006; Hashemi and Lisanti, 2010). Then, the diffusivities are calculated in each direction and the values are put in a 3 by 3 matrix, called diffusion tensor (Ni *et al*., 2006). The diffusion tensor is in the laboratory coordinate and cannot show the dominant diffusion direction and its amplitude. Therefore, it should be transformed into the tissue-based coordinate. In this manner, a mathematical operation, called diagonalization, is performed on each voxel separately. This operation alters every non diagonal elements to zero and yields new non-zero diagonal quantities. The new diagonal elements are called eigenvalues. Eigenvalues are represented by λ (e.g., λ_1, λ_2, λ_3). Each eigenvalue has a corresponding eigenvector. Eigenvectors are represented by ε (e.g., ε_1, ε_2, ε_3). Eigenvalues represent the diffusivities along the three principal diffusion axes in the tissue-based frame of reference. In the case of $\lambda_1 \geq \lambda_2 \geq \lambda_3$ λ_1 is the principal eigenvalue representing the diffusivity along the least restricted direction; e.g., parallel to the myocardial fibers. The eigenvalues are identical in a purely isotropic medium (such as a pericardial cyst) (Raja *et al*., 2011).

Eigenvectors represent the principal diffusion directions relative to the laboratory coordinate. The principal eigenvector corresponds to the main fiber' orientation in a voxel (Basser and Pierpaoli, 2011; Yu *et al*., 2013).

The primary DTI's application is to express the tissue's diffusion anisotropy maps and its microstructures" spatial orientations. Once the diffusion tensor is estimated, it becomes very hard to express the tissues' diffusivities and diffusion anisotropies in an understandable and summarized manner. Therefore, there should be a standard and unique index to indicate the molecular diffusion coefficient and anisotropy in each voxel. There is a variety of indices in DTI. Some of them are popular and clinically feasible, but some of them are not. Here, a brief explanation of the most clinically used indices is given:

Apparent Diffusion Coefficient (ADC): ADC is the average of diffusivities along the scanner's three orthogonal axises (x, y and z). ADC can be mathematically calculated as (Mori and Zhsng, 2006; Soares *et al*., 2013):

$$S_y = S_0 e^{-b_{yy} D_{yy}}$$
$$S_z = S_0 e^{-b_{zz} D_{zz}} \quad (18)$$

$$S_x = S_0 e^{-b_{xx} D_{xx}}$$

If $b_{xx} = b_{yy} = b_{zz} = b$, then

$$ADC = \frac{D_{xx} + D_{yy} + D_{zz}}{3} = \frac{1}{3b} \ln\left[\frac{S_0^3}{S_X S_Y S_Z}\right] \quad (19)$$

Trace: The diagonal axis of any symmetrical matrix is called "Trace". Trace is rotationally invariant and is another common used index in diffusion tensor imaging data interpretation:

$$Trace = D_{xx} + D_{yy} + D_{zz} = 3ADC \quad (20)$$

Fractional Anisotropy (FA): FA determines the magnitude by which the diffusion pattern is anisotropic in a voxel (Soares *et al*., 2013; Yu *et al*., 2013):

$$FA = \sqrt{\frac{1}{2}} \frac{\sqrt{(\lambda_1 - \lambda_2)^2 + (\lambda_2 - \lambda_3)^2 + (\lambda_3 - \lambda_1)^2}}{\sqrt{\lambda_1^2 + \lambda_2^2 + \lambda_3^2}} \quad (21)$$

FA tolerates between 0 and 1. FA = 0 means the diffusion is isotropic and FA = 1 means that the diffusion pattern is completely anisotropic.

Relative Anisotropy (RA): RA is an alternative to FA. It determines the magnitude diffusion anisotropy in a voxel (Mori and Tournier, 2013; Yu *et al*., 2013):

$$RA = \frac{\sqrt{(\lambda_1 - \lambda_2)^2 + (\lambda_2 - \lambda_3)^2 + (\lambda_3 - \lambda_1)^2}}{\sqrt{\lambda_1^2 + \lambda_2^2 + \lambda_3^2}} \quad (22)$$

In contrast with FA, RA tolerates in the range of 0-√2. RA = 0 means isotropic diffusion pattern and the RA =√2 represents a completely anisotropic diffusion pattern in an imaging voxel.

Volume Ratio (VR): VR expresses the ratio of the diffusion ellipsoid volume (with the semi-diameters of λ1, λ2, λ3) to a sphere (with a radius equaling to the average of eigenvalues) (Mori and Tournier, 2013):

$$VR = \frac{\lambda_1 + \lambda_2 + \lambda_3}{\left(\frac{\lambda_1 + \lambda_2 + \lambda_3}{3}\right)^3} \quad (23)$$

The VR = 1 means the diffusion is isotropic and the VR = 0 represents that the diffusion is completely anisotropic in a tissue.

Axial Diffusivity (AD): This index represents the diffusivity along the principal axis of diffusion and is equal to the principal eigenvalue:

$$AD = \lambda_1 \quad (24)$$

Radial Diffusivity (RD): The radial diffusivity is the mean diffusivity perpendicular to the principal axis of diffusion:

$$RD = \frac{\lambda_3 + \lambda_2}{2} \quad (25)$$

Although, the myocardial microstructural orientational information can be fully represented by eigenvectors, there should be some extra standard pre-defined angles to express the myocardial fibers' orientations relative to the heart's standard cylindrical coordinate system. The human heart has three major planes, which are named as the tangent, transverse and the radial planes. The Transverse Plane (TP) is the left/right ventricular standard short-axis plane; the tangent plane is the parallel plane to the epicardial surface (TAP) and the radial plane is the plane extended by the transverse and longitudinal planes (RP) (Jiang *et al*., 2004; Clayton *et al*., 2010).

Helix Angle (HA): HA is defined by the angulation between the first principal eigenvector's projection onto the tangent surface and TP (Jiang *et al*., 2004; Clayton *et al*., 2010). It is usually expressed as -90° to+90°. The HA = +90° means that the fibers are oriented toward the apical region and the HA = -90° indicates that the heart fibers travel toward the cardiac base (Lombaert *et al*., 2012).

Transverse Angle (TA): TA is defined by the angulation between the first principal eigenvector's projection onto the transverse plane and RP. The TA is usually expressed as -90° to +90°. The HA = +90° indicates that the fibers are oriented toward the mid-ventricular cavity and the HA = -90° connotes to the fiber orientations toward the epicardium (Lombaert *et al*., 2012). The FA, MD, ADC, Trace, VR, AD and RD indices are usually represented as grayscale images. Greater values result in more brightness. For instance, areas of brightness on RA and FA mapsindicate anisotropic diffusion. The diffusion anisotropy maps are useful in the investigation of white-matter integrity.

Mathematics: Diffusion tensor imaging assumes that the diffusion follows a Gaussian probability distribution function in every direction. Therefore, the diffusion geometric shape tends to be elliptical. Equation. 9 is always applicable for the isotropic or one-dimensional diffusion measurements. For measuring diffusion in several axises (in any anisotropic materials), Eq. 15 should be altered to Eq. 26:

$$\overline{\left(G(t)dt\right]dt'} \tag{26}$$

Where $\overline{(G(t))dt]}$ is the applied diffusion encoding gradients' profile with the strength of G and the duration of δ. Equation 26 considers the diffusion's directionality by the $\overline{\overline{D}}$ term or the diffusion tensor matrix. If we substitute the parameters of t, t' and t" with the corresponding times of δ or Δ and solve Eq. 26, Eq. 27 will be attained:

$$S = S_0 e^{-b\bar{g}^T\overline{\overline{D}}\bar{g}} \tag{27}$$

Where:

b = The b-value

$\bar{g}$ = The diffusion encoding directions unit vector

$\overline{\overline{D}}$ = Stands for the diffusion tensor

In diffusion tensor imaging, two types of matrices are reconstructed beside the source diffusion weighted images. Those are the b-value and b-vector matrices. The b-value matrix contains the applied diffusion gradient pulses' profiles information (b) and the b-vector matrix returns the information respecting to the applied diffusion directions ($\bar{g}$). Therefore, all of the parameters are known in Eq. 27, except $\overline{\overline{D}}$. $\overline{\overline{D}}$ is the major parameter that must be calculated in DTI.

Firstly, three diffusion gradient pulses are applied in the x, y and z laboratory directions, So that Eq. 27's exponent becomes:

$$\gamma^2G^2\delta^2\left(-\frac{\delta}{3}\right)(100)\begin{pmatrix}D_{xx} & D_{xy} & D_{xz}\\ D_{yx} & D_{yy} & D_{yz}\\ D_{zx} & D_{zy} & D_{zz}\end{pmatrix}\begin{pmatrix}1\\0\\0\end{pmatrix} \tag{28}$$

$$\gamma^2G^2\delta^2\left(-\frac{\delta}{3}\right)(010)\begin{pmatrix}D_{xx} & D_{xy} & D_{xz}\\ D_{yx} & D_{yy} & D_{yz}\\ D_{zx} & D_{zy} & D_{zz}\end{pmatrix}\begin{pmatrix}0\\1\\0\end{pmatrix} \tag{29}$$

$$\gamma^2G^2\delta^2\left(-\frac{\delta}{3}\right)(001)\begin{pmatrix}D_{xx} & D_{xy} & D_{xz}\\ D_{yx} & D_{yy} & D_{yz}\\ D_{zx} & D_{zy} & D_{zz}\end{pmatrix}\begin{pmatrix}0\\0\\1\end{pmatrix} \tag{30}$$

If we solve the above equations and replace into the Eq. 27, the respecting DTI signal equations will change as Eq. 31:

$$\ln\left(\frac{S}{S_0}\right) = -D_{xx}\gamma^2G^2\delta^2\left(\Delta-\frac{\delta}{3}\right) \tag{31}$$

$$\ln\left(\frac{S}{S_0}\right) = -D_{yy}\gamma^2G^2\delta^2\left(\Delta-\frac{\delta}{3}\right) \tag{32}$$

$$\ln\left(\frac{S}{S_0}\right) = -D_{zz}\gamma^2G^2\delta^2\left(\Delta-\frac{\delta}{3}\right) \tag{33}$$

Now, we can calculate the diagonal diffusivities (D_{xx}, D_{yy}, D_{zz}) along the three orthogonal laboratory axises from the Eq. 31-33. To calculate the off-diagonal diffusivities (D_{xy}, D_{xz} and D_{yz}) the diffusion signal must be calculated in the xy, xz and yz directions. In this case, just the b-vector matrices are changed. Therefore, Eq. 27 exponent becomes:

$$\gamma^2G^2\delta^2\left(-\frac{\delta}{3}\right)\begin{pmatrix}\sqrt{\frac{1}{2}} & \sqrt{\frac{1}{2}} & 0\end{pmatrix}\begin{pmatrix}D_{xx} & D_{xy} & D_{xz}\\ D_{yx} & D_{yy} & D_{yz}\\ D_{zx} & D_{zy} & D_{zz}\end{pmatrix}\begin{pmatrix}\sqrt{\frac{1}{2}}\\ \sqrt{\frac{1}{2}}\\ 0\end{pmatrix} \tag{34}$$

$$\gamma^2G^2\delta^2\left(-\frac{\delta}{3}\right)\left(\sqrt{\frac{1}{2}}0\quad\sqrt{\frac{1}{2}}\right)\begin{pmatrix}D_{xx}&D_{xy}&D_{xz}\\D_{yx}&D_{yy}&D_{yz}\\D_{zx}&D_{zy}&D_{zz}\end{pmatrix}\begin{pmatrix}\sqrt{\frac{1}{2}}\\0\\\sqrt{\frac{1}{2}}\end{pmatrix} \quad (35)$$

$$\gamma^2G^2\delta^2\left(-\frac{\delta}{3}\right)\left(0\sqrt{\frac{1}{2}}\quad\sqrt{\frac{1}{2}}\right)\begin{pmatrix}D_{xx}&D_{xy}&D_{xz}\\D_{yx}&D_{yy}&D_{yz}\\D_{zx}&D_{zy}&D_{zz}\end{pmatrix}\begin{pmatrix}0\\\sqrt{\frac{1}{2}}\\\sqrt{\frac{1}{2}}\end{pmatrix} \quad (36)$$

If we solve Eq. 34-36 and replace them into the Eq. 27, Eq. 37 are achieved:

$$\ln\left(\frac{S}{S_0}\right)=-\gamma^2G^2\delta^2\left(\Delta-\frac{\delta}{3}\right)\left(\frac{1}{2}D_{xx}+D_{xy}+D_{yy}\right) \quad (37)$$

$$\ln\left(\frac{S}{S_0}\right)=-\gamma^2G^2\delta^2\left(\Delta-\frac{\delta}{3}\right)\left(\frac{1}{2}D_{xx}+D_{xz}+\frac{1}{2}D_{yy}\right) \quad (38)$$

$$\ln\left(\frac{S}{S_0}\right)=-\gamma^2G^2\delta^2\left(\Delta-\frac{\delta}{3}\right)\left(\frac{1}{2}D_{yy}+D_{yz}+\frac{1}{2}D_{zz}\right) \quad (39)$$

Now, the diffusion tensor's off-diagonal diffusivities can be computed. By the computation of all the diffusivities, the diffusion tensor matrix can be fully defined as:

$$\overline{\overline{D}}=\begin{bmatrix}D_{xx}&D_{xy}&D_{xz}\\D_{yx}&D_{yy}&D_{yz}\\D_{zx}&D_{zy}&D_{zz}\end{bmatrix} \quad (40)$$

Now, the diagonalization operation can be performed on the diffusion tensor. It results in a diagonal matrix. The diagonal matrix is equivalent to the diffusion tensor but its elements are completely different. The new matrix's off-diagonal elements are zero and its diagonals are completely different. The explanation of diagonalization is out of this article's scope and explained comprehensively in every linear algebra mathematical books. Simply, the diagonalization is the mathematical operation that is used to change the laboratory coordinate into the tissue-based frame of reference. It results in three major quantities called eigenvalues and three major angles called eigenvectors. The eigenvectors represent the principal diffusion directions relative to the laboratory coordinate and the eigenvalues indicate the tissues' diffusivities along eigenvectors (Basser *et al*., 1994; Basser *et al*., 2000; Basser and Jones, 2002).

In *in-vivo* cDTI, the maximum possible number of applied diffusion sensitizing directions should be kept least to maintain the acquisition time logically short. By this small number of diffusion encoding directions, a precise microstructural mapping seems to be impossible while the myocardial tissue consists of a lot of crossing fibers, especially in the infarcted regions (Sosnovik *et al*., 2009). Consequently, there is a growing interest to develop higher angular resolution techniques; e.g. High Angular Resolution Diffusion Imaging (HARDI) Q-ball Imaging and Diffusion Spectrum Imaging (DSI), etc. The cardiological application of higher order diffusion MRI seems to be impractical with today's technology due to the techniques' prolonged acquisition time.

RESULTS AND DISCUSSION

Common pulse sequences: Cardiac diffusion-weighted imaging is a challenging field and will encounter many obstacles in its path to the clinics. Its most common drawbacks are:

Cardiac pulsation: Heart is a mobile organ. Its architecture changes during each cycle (P-wave, QRS complex and T-wave). Consequently, different restriction patterns appear in systolic and diastolic phases (Ferreira *et al*., 2014; McGill *et al*., 2016). Besides, the cardiac arrhythmia limits the image quality and make it prone to heavy motion artifacts.

Cardiac short T2 relaxation time: The myocardial T2 relaxation time is very short (T2≈40 ms) in comparison with other organs (Scholz *et al*., 1989; Stanisz *et al*., 2005) thus, an extreme short Echo Time (TE) pulse sequence should be designed to reduce the T2 decay contributions to NMR signal.

Local different magnetic susceptibility effects: Heart is surrounded by lungs. The pulmonary alveolar tissue is full of air and destroys the local magnetic field homogeneity. Therefore, less sensitive pulse sequences should be applied in the clinical practice (Ferreira *et al*., 2013). Hence, the simple PGSE method is not practical due to its sensitivity to magnetic field inhomogeneity and Eddy artifacts. It has a relatively long TE. Some of the most common alternative sequences to PGSE are:

Diffusion Encoded Stimulated Echo (DSTE): In the DSTE method, three 90° RF pulses are transmitted to the patient during two cardiac cycles. The two first RF pulses are sent at the same cycle but the last one in transmitted during the next heart beat. The diffusion encoding gradients are applied after the 1st and 3rd RF pulses. Figure 5 helps to a better understanding of the underlying mechanism (Edelman *et al*., 1994; Reese *et al*., 1995; Nielles-Vallespin *et al*., 2013; Von Deuster *et al*., 2015).

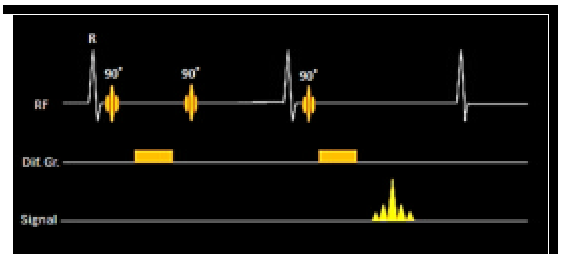

Fig. 5: A schematic diagram of the diffusion-encoded stimulated echo pulse sequence. During the first RF pulse transmission, the magnetization flips into the xy plane. At the time of RF cease, the magnetization decreases slightly due to the spin-spin interaction and longitudinal recovery. When the second RF pulse is applied, the remained transverse magnetization returns to the longitudinal axis and the relaxed portion of nuclei are transferred into the transverse plane again. By the application of the third RF pulse, all the longitudinal magnetization flips into the transverse plane and produces a Hahn's signal. The diffusion encoding gradients are applied after the first and third RF pulses.

Advantages: The DSTE method does not require any extra and high-performance gradient hardware. It can almost be applied on any clinical scanners. Because of long Δ gradients interval, higher b-values can be achieved at low gradient amplitudes and strengths. The DSTE method's echo time is much shorter than the myocardial T2 relaxation time; thus, its T2 contrast contamination is little. Its sensitivity to magnetic susceptibility artifact is low (Nguyen *et al*., 2015).

Disadvantages: After the third RF pulse application, a crusher gradient is needed to destroy the Free Induction Decay (FID) signal. The crusher gradient sensitizes the signal to diffusion weighting. Therefore, it seems impossible to acquire b = 0 s/mm^{-2} images by the DSTE approach. The DSTE method is so sensitive to motion and cardiac arrhythmias while all the three RF pulses should be transmitted to the same slice position to produce a beneficial, signal.

Velocity Compensated PGSE (VC-PGSE): The VC-PGSE pulse sequence is a modification of the conventional Stejskal-Tanner technique. It is applied during a cardiac cycle and permits a breath-hold single-shot data acquisition. The method applies a pair of bipolar diffusion

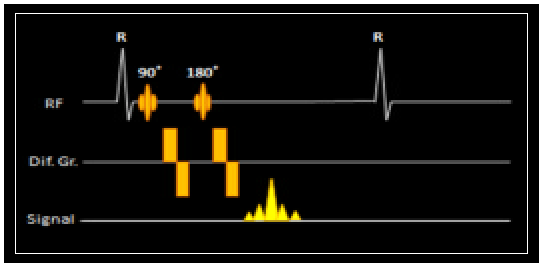

Fig. 6: A schematic diagram of the velocity compensated PGSE (VC-PGSE) method. In this technique, two pairs of bipolar gradients are appended to the conventional Stejskal-Tanner method before and after the 180° RF pulse

encoding gradients before and after the 180° RF pulse in the mid-systolic phase. The VS-PGSE method compensates for the first-order blood flow artifact and increases the diffusion gradients' revenue (Fig. 6) (Gamper *et al*., 2007; Froeling *et al*., 2015):

Advantages: The VC-PGSE method is less sensitive to cardiac motion and provides a shorter TE in comparison with DSTE. Its time of acquisition is relatively short and enables high-resolution cDTI whole heart tractography in-vivo.

Disadvantages: The method heavily depends on the gradient hardware performance and can be used in the clinical scanners with the maximum gradient strength of 80 mT/m. Its sensitivity to noise is more that the DSTE method.

Acceleration Compensated Spin-Echo (AC-SE): The AC-SE method uses a pair of assymetrical bipolar diffusion encoding gradients before and after the 180° RF pulse (similar to VC-PGSE) but the negative lobe's elapsed time duration is more than the positive lobe's duration. AC-SE compensates both the first and second-order blood flow effects on intravoxel dephasing; thus, increases the cDTI's SNR, CNR and reproducibility during a cardiac cycle (Fig. 7) (Froeling *et al*., 2014; Stoeck *et al*., 2016):

Advantages: The AC-SE method's SNR and CNR is in an acceptable range. It can produce high-quality images from the entire cardiac cycle, especially at the early systolic and diastolic phases.

Disadvantages: There is a requirement for high-performance gradient hardware similar to the

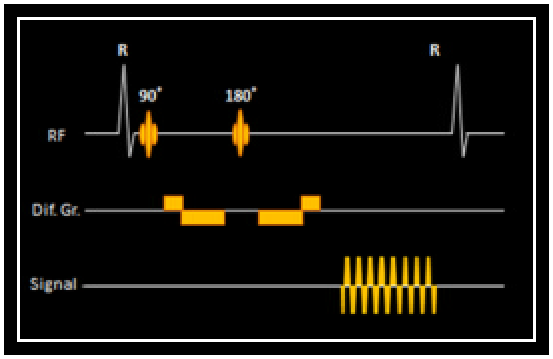

Fig. 7: A schematic diagram of the acceleration Compensated Spin-Echo (AC-SE) method. It is a simple spin echo sequence conjugated with a pair of bipolar gradients before and after the 180° RF pulse. The negative lobe's elapsed time duration is more than the positive lobe's duration. The method is attached with an EPI readout acquisition technique to reduce the scan time

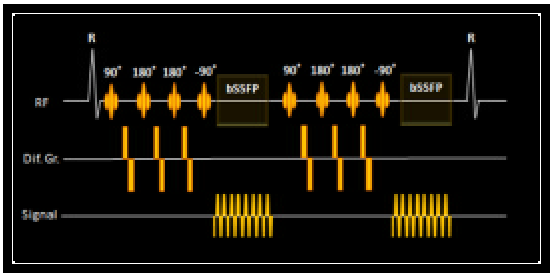

Fig. 8: A schematic diagram of the Segmented Diffusion Sensitizing Driven-Equilibrium bSSFP (SDE-bSSFP) pulse sequence. In SDE-bSSFP, several bSSFP data acquisitions are accomplished during each cardiac cycle. Before each signal acquisition, a preparatory driven-equilibrium twice-refocused spin echo sequence is applied which results in diffusion sensitization

VC-PGSE method. The method's acquisition time is longer than the VC-PGSE method and cannot provide high-resolution whole heart images in a logical acquisition time.

Segmented Diffusion Sensitizing Driven-Equilibrium bSSFP (SDE-bSSFP): This sequence is a combination of several intermittent bSSFP readout techniques with a diffusion sensitized driven equilibrium twice-refocused spin echo preparatory phase at each interval. On the other hand, there are two or more bSSFP signal acquisition segments at each R-R interval. Before each bSSFP segment, a diffusion sensitized preparatory phase is

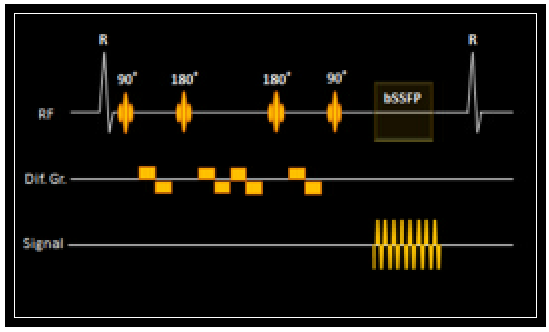

Fig. 9: A schematic diagram of the Acceleration Compensation Balanced Steady-state Free Precession (AC-bSSFP) pulse sequence. It is similar to the SDE-bSSFP method but there is a slight difference in the numbers of the diffusion sensitizing gradients to reduce its sensitivity to second-order blood flow intravoxel dephasing

applied. In the depth of each preparatory phase, a diffusion sensitized Twice-Refocused Spin-Echo (TRSE) sequence exists. At the end of each TRSE, there is an implementation of a tip-up RF pulse with a spoiler gradient to return thetransverse magnetization into the longitudinal axis and dephase the remnant transverse phase coherence. SDE-bSSFP is insensitive to small bulk motions (Fig. 8) (Jeong *et al*., 2003).

Advantages: It compensates small motion artifacts (e.g., cerebrospinal fluid artifact) and do not require robust phase correction algorithms. It can be accomplished two- or three-dimensionally and results in high-resolution images. The SNR is acceptable and suffers less from magnetic susceptibility artifact.

Disadvantages: The SDE-bSSFP method cannot eliminate accelerated blood flow effects on intravoxel phase coherence and thereby cannot be utilized in different cardiac functional phases. It requires high gradient capabilities.

Acceleration Compensation Balanced Steady-State Free Precession (AC-bSSFP): The AC-bSSFP method is similar to the SDE-bSSFP method though there is a single data acquisition segment at each R-R interval. The preparatory phase is applied during the mid-diastolic phase and similar to the SDE-bSSFP method's preparatory phase; the RF pulses' structures and characteristics are the same but 4 pairs of non-uniform diffusion sensitizing gradients are applied instead of three (in contrast with the SDE-bSSFP method) (Fig. 9) (Nguyen *et al*., 2014).

Advantages: The method compensates the small motion and accelerated blood flow artifacts because of its excellent design. It results in high-resolution three-dimensional images in a logical scan time by the respiratory navigation technique. Its SNR is in an acceptable range and overcomes pulmonary magnetic susceptibility effects on local shimming.

Disadvantages: The method requires high slew rate gradient hardware and can only be implemented in the diastolic cardiac phase. It is less reproducible in tachycardia and less efficient at short ventricular diastoles.

Clinical applications

Case reports: Various primary and secondary neoplastic tissues can involve the human heart. Studies have shown that the cardiac DWI helps clinicians to characterize and differentiate the pericardial lesions types greatly. In 2011, Raja *et al*. (2011) described the role of ADC maps in the congenital pericardial cysts diagnosis and its differentiation from other types of lesions. They reported that the congenital pericardial cystic lesions appear bright on ADC maps. Ozmen *et al* (2015) also reported the power of cDWI and ADC maps in the primary pericardial synovial sarcoma tumor diagnosis which is known as a rare pericardial lesion. Okayama *et al*. (2009) published a case report which represented the low b-value cDWI's high diagnostic power in the infarct-related myocardial edema detection. They believed that the low b-value diffusion imaging has a higher sensitivity to edema than the conventional T2w images and can depict it more accurately.

Research: Most of the cDWI investigations are held *ex-vivo*. There is a lack of *in-vivo* studies to explore the cDWI's diagnostic role in the different cardiomyopathy types. Most of the investigations are focused on acute/sub-acute/chronic Myocardial Infarctions (MI) or Hypertrophic Cardio Myopathy (HCM).

Hypertrophic cardiomyopathy: Nguyen *et al*. (2015) studied the cDWI's diagnostic value in the patients with the absolute diagnosis of HCM. They compared the diffusion-weighted images with the Late Gadolinium Enhancement (LGE), T1 relaxometry (T1r) and Extra Cellular Volume (ECV) images. They announced that the ADC values in fibrotic regions increased significantly in comparison with the non-fibrotic myocardium. They also reported the ADC map's sensitivity, specificity, negative predictive value, positive predictive value and accuracy to be 80, 85, 85, 81 and 83% respectively. In conclusion, Nguyen *et al*. (2015) stated that the cardiac DWI is a sensitive tool in diffuse myocardial fibrosis detection and can be an alternative technique to characterize myocardial fibrosis in HCM. Wu *et al*. (2016) made an investigation on HCM too. They studied the quantitative cardiac DWI's diagnostic power in comparison with the T1 relaxometry method. They reported that the diseased myocardial ADC value is significantly higher than the healthy/normal myocardial values. They also reported an equal diagnostic power between the ADC maps, T1 relaxometry and extracellular volume imaging methods to differentiate the normal from fibrotic tissues. In the conclusion, they stated that the heart DWI may be an alternative method to T1 mapping and ECV in the HCM evaluations (Wu *et al*., 2016). Besides the ADC maps, the hypertrophied myocardial integrity and microstructures can be evaluated by cDTI. Studies have shown that the myocardial integrity and arrangement degenerates in HCM in comparison with the normal hearts (Bacharova and Ugander, 2014).

Myocardial Infarction: Laissy *et al*.(2013) conducted a pilot study and investigated the cardiac DWI's diagnostic power to differentiate the acute, sub-acute and chronic MIs from each other. They reported no significant differences between the ADC values in acute and sub-acute MIs. In contrasts, they stated a meaningful difference between the acute and chronic Mis ADCs ($p < 0.001$). Laissy *et al*. (2009) concluded that the cardiac DWI is a sensitive technique to diagnose the acute myocardial infarctions and an excellent method to differentiate it from the chronic ones. Teraoka *et al*. (2008) made a comparison between the cardiac diffusion-weighted and late gadolinium enhancement imaging techniques in the acute myocardial infarction and reported a significant linear correlation between the LGE and DWI hyperenhancement patterns in acute MIs Kloeckner *et al*. (2011) evaluated the correlation between the Left Ventricular Ejection Fraction (LVEF) recovery and the cardiac diffusion weighted signal as a predictor after acute MI. They reported that the $b = 50$ s/mm^{-2} images provide an accurate assessment of the myocardial injury and might be a good predictor of the LVEF recovery. Wu *et al*. (2006) led a research about the role of cDTI in the post-MI myocardial fiber architecture remodeling assessments. They accomplished cDTI on 37 MI diagnosed patients. They calculated heart FA, HA and ADC maps and computed the values in the infarcted and healthy remote zones. Wu et al reported a significantly increased ADC, decreased FA and a strongly decreased right-handed subendocardial fiber orientation in the diseased regions. They concluded that the cDTI might be

a strong imaging technique to diagnose the chronic myocardial infarctions by new indices and may open a deep insight into the myocardial mechanics and structural remodeling mechanisms post-infarctions (Wu *et al*., 2006). DWI can also be a sensitive technique to diagnose the post-infarctions myocardial edema (Okayama *et al*., 2007; Kociemba *et al*., 2013a,b). Kociemba *et al*. (2013) evaluated the role of cardiac DWI for the edema detection in acute MIs and compared their results with the standard T2w images. They reported that the DWI's sensitivity was similar to the standard T2w images in all myocardial regions except the inferior wall, where the standard T2w and DWI's sensitivities were 46 and 85% respectively. In conclusion, they recommended the cardiac DWI as a novel and excellent technique to diagnose myocardial acute injuries, especially in the patients with the slow flow artifacts.

Myocarditis: Myocarditis is an inflammatory disease and outcomes to myocardial edema. Kociemba *et al*. (2015) showed a strong correlation between the low b-value ($b = 50$ s/mm^{-2}) diffusion-weighted images and the Lake Louise criteria myocarditis assessment. They reported that the signal intensity is significantly higher in all the edematous regions. They also reported a higher Contrast to Noise Ratio (CNR) value in the cardiac diffusion-weighted images than the standard T2w results. Higher CNR makes the qualitative assessments more accurate (Kociemba *et al*., 2015). Potet *et al*. (2013) led a research and demonstrated a strong correlation between the cDWI's low b-value and LGE images to detect the edema in acute myocarditis. They also declared that the cardiac DWI's sensitivity and diagnostic accuracy are significantly stronger than the conventional T2wimaging. In conclusion, they recommended the cardiac DWI as an alternative tool to the standard Short Tau Inversion Recovery (STIR) T2-weighted imaging in the acute myocarditis assessments (Potet *et al*., 2013).

Unfortunately, few studies have been conducted to assess the cDWI's role in other cardiomyopathies; e.g. Restrictive Cardio Myopathy (RCM) Non-compaction Cardiomyopathy (NCMP) Arrhythmogenic Right Ventricular Dysplasia (ARVD) Dilated Cardiomyopathy (DCM) etc. As there is always a structural/functional correlation in different cardiomyopathies, cDTI can become a novel and useful technique to study the human's different heart diseases clinically.

Cardiac DWI has confronted many challenges to become feasible in cardiac practice. The most serious limitation is the lack of a practical pulse sequence. Most of the introduced pulse sequences are time-consuming and thereby not suitable for clinical settings. Some of them require high-performance gradient hardware with rapid slew rates and drastic strengths. Briefly, a clinically suitable pulse sequence should fulfill the criteria:

- High sensitivity, specificity and accuracy to different pathologies and microstructural changes
- An acceptable degree of reproducibility and repeatability
- Least sensitivity to distortion and motion artifacts
- Sensibly short acquisition times (to the extent of a single-shot breath-hold acquisition)
- Providing the highest possible SNR and CNR

As mentioned previously, most of the cDWI pulse sequences require special gradient coils hardware to compensate the second order blood flow intravoxel dephasing and reduce the acquisition time. Most of the cDWI sequences are sensitive to either inter- or intra-shot motion artifacts. Motion often arises from three sources, the patient bulk movement, cardiac and respiratory motions and table vibration. These days, there are various prospective and retrospective motion correction methods available to reduce the patient's motion artifact inside of the MRI scanner. Generally, the prospective methods acquire the patient's motions patterns during or prior to the main readout time to compile them into the final images, while the retrospective methods use different types of post- processing algorithms to compensate the patient's involuntary motions artifacts.

Patient's bulk motion artifacts: The bulk motion artifacts can be eliminated with improved patient cooperation or the application of the sedative pharmaceuticals based on the established guidelines (Arlachov and Ganatra, 2014; Moran *et al*., 2013). The use of a single-shot pulse sequence and a parallel technique together can help to freeze the patient's motion. The parallel acquisition technique can make the diffusion weighted images less sensitive to motion artifact by making a dramatical decrease in the acquisition time at the cost of increasing the image noise (Holdsworth *et al*., 2009). Although, most of the studies have used the parallel technique during their investigations, none of them has delineated the effects of different parallel techniques on the final calculated anisotropy maps. Most of the cDWI/cDTI designed pulse sequences are based on the respiratory navigation technique and take a long time to image the whole heart, thereby increasing the likelihood of the patient movements.

Cardiac/respiratory motion artifacts: Electro Cardio Graphic (ECG) gating can almost compensate most of the

pulsation artifacts, except in the case of arrhythmias. As mentioned earlier, the myocardial microstructure changes during cardiac systoles and diastoles. This issue necessitates us to determine a standard ECG phase for imaging. The determination of a certain gating phase improves our ability to perform intra- and inter-subject analysis. Studies have shown that the R-R time interval significantly affects the anisotropic indices (McGill *et al*., 2016). Arrhythmia is the major problem in cardiac MRI. Even, the routine clinical retrospective/prospective pulse sequences cannot fully reject the sudden arrhythmia's artifacts in the reconstructed images. Yet, no studies have been launched to investigate the arrhythmogenic pulsations' effects on the diffusion anisotropic maps.

As well as the cardiac pulsation artifacts, respiratory motion can disturb the image quality so much. Most of the designed pulse sequences use the respiratory navigation technique to compensate the respiratory motion artifacts in the final DW images. The respiratory navigation technique is protracted and its long acquisition time is in contrast with the cardiac imaging's essence. In the routine clinical cardiac MRI, most of the stationary pulse sequences are single-shot to eliminate the patient's respiration effects on image quality. Theses sequences are so useful in uncooperative patients. cDWI will have a remarkable role in the patients with acute MIs; thus, the imaging time is a critical factor in the clinical practice. Consequently, the conjugation of the diffusion-weighted pulse sequences with the navigation technique will be troublesome.

Table vibration artifacts: Table vibration artifacts are induced by the strong fast-switching diffusion-weighted gradients. A short-term solution to the table vibration artifact is to decrease the diffusion-weighting gradient's amplitude. This can be done either by prolonging the diffusion gradient pulse duration while keeping the same b-value (results in a longer TE which degrades the SNR) (Farrell *et al*. 2007; Choi *et al*., 2011; Polders *et al*., 2011) or overally the use of lower b-values at the cost of lesser diffusion weighting. Unfortunately, increasing the diffusion gradient's duration is impractical in cardiac imaging due to the necessary ECG-gating. So, there should be a study to search for another solution to this problem.

Signal to noise ratio: Image noise can influence anisotropy maps. Maintaining the SNR in an acceptable range is very crucial in cDTI. Poor SNR results into information bias. Farrel *et al*. (2007) reported that the FA maps experience an upward bias if the SNR lessens (Seo *et al*., 2012). Achieving the highest possible SNR is pivotal for successful DTI studies because the noise tends to cause an overestimation and underestimation of the major and minor eigenvalues respectively. In addition, noise affects the real eigenvectors to a great extent (Basser and Pajevic, 2000). Studies showed that STEAM based sequences provide better SNR than the spin echo based methods when the high b-values are needed (Zhang *et al*., 2008). The other key parameter that influences SNR is the b-value. High b-values reduce the SNR. There should be a balance between the number of the diffusion gradient directions the b-values for acquiring an almost noise free image. The number of the diffusion encoding directions can influence the FA values, while the b-value usually affects the MD maps (Reese *et al*., 1995).

Image distortion: Unfortunately, the rapid pulse sequences suffer from the image blurring, eddy current and magnetic field inhomogeneity artifacts (Jones and Cercignani, 2010). Both of the Eddy current and magnetic field inhomogeneity artifacts can warp the image data, thereby distracting the real image's spatial information (Jezzard and Balaban, 1995; Haselgrove and Moore, 1996). The Eddy distortion artifact misaligns the DW image series and results in the eigenvalues and eigenvectors miscomputation (Haselgrove and Moore, 1996; Jezzard *et al*., 1998). In some literature, it is recommended to use the twice-refocused PGSE pulse sequence for *ex-vivo* studies due to its little sensitivity to distortion artifacts (Reese *et al*., 2003).

Sequence parameters: Studies have shown that the diffusion anisotropic maps are heavily dependent on the implemented pulse sequences and selected parameters. For example, a recent study by Kim *et al*. (2015) demonstrated that both of the FA and ADC maps are significantly correlated with echo time, SENSE factor and b-value. They also showed a significant correlation between the number of the diffusion encoding directions and FA values. The scanner's magnetic field can influence the isotropic indices too. Huistman *et al*. (2006) reported that the ADC values can be significantly lower at 3.0 Tesla imaging scanners than 1.5 Tesla. They also proclaimed that the FA values are significantly higher at 3.0 Tesla scanners. Even the image resolution can affect the anisotropy maps. Some studies demonstrated that the FA maps can be affected by the spatial resolution too (Santarell *et al*., 2010)". The optimal b-value for cardiovascular DWI is still unknown. There should be a broad investigation to establish the most optimal b-value for cardiovascular studies. Besides, the optimal number of diffusion gradient directions is also unclear in cDTI.

Unfortunately, few studies have been carried out to discover the most appropriate available pulse sequences in cDWI. However, it seems that none of the introduced sequences satisfies the above criteria and sounds to be practical by today's technology. Briefly, cDWI and cDTI has not been ready to enter the routine clinical practice yet.

CONCLUSION

Cardiac diffusion-weighted imaging is a novel technique that enables the clinicians to assess different types of cardiomyopathies. This technique eliminates the administration of contrast agents, thereby gaining a broad application in the patients with renal failure. The cDWI is technically challenging and requires high-performance types of gradient hardware. Cardiac DWI requires different pulse sequence diagrams than the intracranial diffusion-weighted imaging (with high reproducibility values) to overcome the cardiac imaging's limitations. In the recent years, the motion and accelerated blood flow compensated pulse sequences have been designed to improve the cDWI/cDTI related image qualities and accuracies. cDTI is more accurate than the cDWI due to its number of diffusion encoding directions and resulting anisotropy maps, but it is time-consuming and should be coupled with the respiratory navigation technique. The role of cDWI/cDTI is unclear in the different heart diseases and there should be more investigations on its clinical transition. In conclusion, the clinical cDWI is at its inception and has a long way to be admitted in the routine cardiovascular MRI.

REFERENCES

Alexander, A.L., J.E. Lee, M. Lazar and A.S. Field, 2007. Diffusion tensor imaging of the brain. Neurotherapeutics, 4: 316-329.

Arlachov, Y. and R.H. Ganatra, 2014. Sedation anaesthesia in paediatric radiology. Br. J. Radiol., 85: e1018-e1031.

Bacharova, L. and M. Ugander, 2014. Left ventricular hypertrophy: The relationship between the electrocardiogram and cardiovascular magnetic resonance imaging. Ann. Noninvasive Electrocardiol., 19: 524-533.

Basser, P.J. and C. Pierpaoli, 2011. Microstructural and physiological features of tissues elucidated by quantitative-diffusion-tensor MRI. J. Magn. Reson., 213: 560-570.

Basser, P.J. and D.K. Jones, 2002. Diffusion-tensor MRI: Theory, experimental design and data analysis-a technical review. NMR. Biomed., 15: 456-467.

Basser, P.J. and S. Pajevic, 2000. Statistical artifacts in diffusion tensor MRI (DT-MRI) caused by background noise. Magn. Reson. Med., 44: 41-50.

Basser, P.J., J. Mattiello and D. LeBihan, 1994 a. Estimation of the effective self-diffusion tensor from the NMR spin echo. J. Magn. Reson.: Ser. B, 103: 247-254.

Basser, P.J., J. Mattiello and D. LeBihan, 1994b. MR diffusion tensor spectroscopy and imaging. Biophys. J., 66: 259-267.

Basser, P.J., S. Pajevic, C. Pierpaoli, J. Duda and A. Aldroubi, 2000. *In vivo* fiber tractography using DT-MRI data. Magn. Reson. Med., 44: 625-632.

Berman, J.I., M.R. Lanza, L. Blaskey, J.C. Edgar and T.P.L. Roberts, 2013. High angular resolution diffusion imaging probabilistic tractography of the auditory radiation. Am. J. Neuroradiol., 34: 1573-1578.

Bloch, F., 1946. Nuclear induction. Phys. Rev., 70: 460-474.

Chenevert, T.L., J.A. Brunberg and J.G. Pipe, 1990. Anisotropic diffusion in human white matter: Demonstration with MR techniques *in vivo*. Radiology, 177: 401-405.

Choi, S., D.T. Cunningham, F. Aguila, J.D. Corrigan and J. Bogner *et al*., 2011. DTI at 7 and 3 T: Systematic comparison of SNR and its influence on quantitative metrics. Magn. Reson. Imaging, 29: 739-751.

Clayton, R.H., S. Abdalhamid, R. Bloor, G. Kyprianou and K. Kotagiri *et al*., 2010. Transmural changes in fibre helix angle in normal and failing canine ventricles. Proceedings of a Meetings on Computing in Cardiology, September 26-29, 2010, Belfast, UK., pp: 915-918.

Conturo, T.E., N.F. Lori, T.S. Cull, E. Akbudak and A.Z. Snyder *et al*., 1999. Tracking neuronal fiber pathways in the living human brain. Proc. Natl. Acad. Sci., 96: 10422-10427.

Edelman, R.R., J. Gaa, V.J. Wedeen, E. Loh, J.M. Hare, P. Prasad and W. Li, 1994. *In vivo* measurement of water diffusion in the human heart. Magn. Reson. Med., 32: 423-428.

Einstein, A., 1956. Investigations on the Theory of the Brownian Movement. 1st Edn., Dover Publications, USA., ISBN-10: 0486603040.

Eyal, E., M. Shapiro-Feinberg, E. Furman-Haran, D. Grobgeld and T. Golan *et al*., 2012. Parametric diffusion tensor imaging of the breast. Invest. Radiol., 47: 284-291.

Farrell, J.A., B.A. Landman, C.K. Jones, S.A. Smith and J.L. Prince *et al*., 2007. Effects of signal-to-noise ratio on the accuracy and reproducibility of diffusion tensor imaging-derived fractional anisotropy, mean diffusivity and principal eigenvector measurements at 1.5 T. J. Magn. Reson. Imaging, 26: 756-767.

Ferreira, P.F., P.D. Gatehouse, R.H. Mohiaddin and D.N. Firmin, 2013. Cardiovascular magnetic resonance artefacts. J. Cardiovasc. Magn. Reson., Vol. 15. 10.1186/1532-429X-15-41

Ferreira, P.F., P.J. Kilner, L.A. McGill, S. Nielles-Vallespin and A.D. Scott *et al*., 2014. *In vivo* cardiovascular magnetic resonance diffusion tensor imaging shows evidence of abnormal myocardial laminar orientations and mobility in hypertrophic cardiomyopathy. J. Cardiovasc. Magn. Reson., Vol. 16. 10.1186/s12968-014-0087-8

Fick, A., 1855. V on liquid diffusion. London Edinburgh Dublin Philos. Mag. J. Sci., 10: 30-39.

Filippi, C.G., A.M. Ulug, E. Ryan, S.J. Ferrando and W. van Gorp, 2001. Diffusion tensor imaging of patients with HIV and normal-appearing white matter on MR images of the brain. Am. J. Neuroradiol., 22: 277-283.

Froeling, M., G.J. Strijkers, A.J. Nederveen and P.R. Luijten, 2015. Whole heart DTI using asymmetric bipolar diffusion gradients. J. Cardiovasc. Magn. Reson., Vol. 17. 10.1186/1532-429X-17-S1-P15 .

Froeling, M., G.J. Strijkers, A.J. Nederveen, S.A. Chamuleau and P.R. Luijten, 2014. Feasibility of *in vivo* whole heart DTI and IVIM with a 15 minute acquisition protocol. J. Cardiovasc. Magn. Reson., Vol. 16. 10.1186/1532-429X-16-S1-O15

Gamper, U., P. Boesiger and S. Kozerke, 2007. Diffusion imaging of the *in vivo* heart using spin echoes-considerations on bulk motion sensitivity. Magn. Reson. Med., 57: 331-337.

Gillard, J.H., A.D. Waldman, P.B. Barker and D.K. Jones, 2005. Fundamentals of Diffusion MR Imaging. In: Clinical MR Neuroimaging (Diffusion, Perfusion and Spectroscopy), Gillard, J.H., A.D. Waldman and P.B. Barker (Eds.). Cambridge University Press, New York, pp: 54-85.

Gupta, A., G.K. Malik, S. Saksena and R.K. Gupta, 2006. MR demonstration of complete cerebellar and corpus callosum agenesis. Pediatr. Neurosurg., 43: 29-31.

Gupta, R.K., K.M. Hasan, A.M. Mishra, D. Jha, M. Husain, K.N. Prasad and P.A. Narayana, 2005. High fractional anisotropy in brain abscesses versus other cystic intracranial lesions. Am. J. Neuroradiol., 26: 1107-1114.

Gupta, S.S., Z.M. Patel and B.K. Misra, 2008. Pictorial essay: Neurosurgical application and physics of diffusion tensor imaging with 3D fiber tractography. Indian J. Radiol. Imag., 18: 37-44.

Hagmann, P., L. Jonasson, P. Maeder, J.P. Thiran, V.J. Wedeen and R. Meuli, 2006. Understanding diffusion MR imaging techniques: From scalar diffusion-weighted imaging to diffusion tensor imaging and beyond. Radiographics, 26: S205-S223.

Hall, J.E. and A.C. Guyton, 2011. Guyton and Hall Textbook of Medical Physiology. 12th Edn., Saunders/Elsevier, USA., ISBN: 9781416045748, Pages: 1091.

Haselgrove, J.C. and J.R. Moore, 1996. Correction for distortion of echo-planar images used to calculate the apparent diffusion coefficient. Magn. Reson. Med., 36: 960-964.

Hashemi, R.H. and C.J. Lisanti, 2010. MRI: The Basics. 3rd Edn., Lippincot Williams amd Wilkins, China.

Holdsworth, S.J., S. Skare, R.D. Newbould and R. Bammer, 2009. Robust GRAPPA-accelerated diffusion-weighted readout-segmented (RS)-EPI. Magn. Reson. Med., 62: 1629-1640.

Huisman, T.A., T. Loenneker, G. Barta, M.E. Bellemann, J. Hennig, J.E. Fischer and K.A. Il'yasov, 2006. Quantitative diffusion tensor MR imaging of the brain: Field strength related variance of Apparent Diffusion Coefficient (ADC) and Fractional Anisotropy (FA) scalars. Eur. Radiol., 16: 1651-1658.

Jeong, E.K., S.E. Kim and D.L. Parker, 2003. High-resolution diffusion-weighted 3D MRI, using diffusion-weighted driven-equilibrium (DW-DE) and multishot segmented 3D-SSFP without navigator echoes. Magn. Reson. Med., 50: 821-829.

Jezzard, P. and R.S. Balaban, 1995. Correction for geometric distortion in echo planar images from B0 field variations. Magn. Reson. Med., 34: 65-73.

Jezzard, P., A.S. Barnett and C. Pierpaoli, 1998. Characterization of and correction for eddy current artifacts in echo planar diffusion imaging. Magn. Reson. Med., 39: 801-812.

Jiang, Y., K. Pandya, O. Smithies and E.W. Hsu, 2004. Three-dimensional diffusion tensor microscopy of fixed mouse hearts. Magn. Reson. Med., 52: 453-460.

Jones, D.K. and M. Cercignani, 2010. Twenty-five pitfalls in the analysis of diffusion MRI data. NMR Biomed., 23: 803-820.

Kastrup, O., I. Wanke and M. Maschke, 2005. Neuroimaging of infections. NeuroRx, 2: 324-332.

Kim, S.J., C.G. Choi, J.K. Kim, S.C. Yun, G.H. Jahng, H.K. Jeong and E.J. Kim, 2015. Effects of MR parameter changes on the quantification of diffusion anisotropy and apparent diffusion coefficient in diffusion tensor imaging: Evaluation using a diffusional anisotropic phantom. Korean J. Radiol., 16: 297-303.

Kloeckner, M., P. Lim, D. Hayat, P. Gueret, A. Rahmouni and J.F. Deux, 2011. Diffusion weighted magnetic resonance imaging and LVEF recovery after acute myocardial infarction. Arch. Cardiovasc. Dis. Suppl., 3: 4-4.

Kociemba, A., J. Rajewska-Tabor, M. Lanocha, M. Janus, A. Siniawski, K. Karmelita-Katulska and M. Pyda, 2015. Detection of myocardial edema with diffusion weighted imaging in patients with acute myocarditis. J. Cardiovasc. Magn. Reson., Vol. 17. 10.1186/1532-429X-17-S1-P331

Kociemba, A., M. Lanocha, K. Katulska, A. Siniawski, M. Janus and M. Pyda, 2013a. A comparision of oedema detection with diffusion-weighted imaging and T2-STIR imaging in patients with acute myocardial infarction. J. Cardiovasc. Magn. Reson., Vol. 15. 10.1186/1532-429X-15-S1-P25

Kociemba, A., M. Pyda, K. Katulska, M. Lanocha, A. Siniawski, M. Janus and S. Grajek, 2013b. Comparison of diffusion-weighted with T2-weighted imaging for detection of edema in acute myocardial infarction. J. Cardiovasc. Magn. Reson., Vol. 15. 10.1186/1532-429X-15-90

Krageloh-Mann, I. and V. Horber, 2007. The role of magnetic resonance imaging in elucidating the pathogenesis of cerebral palsy: A systematic review. Dev. Med. Child Neurol., 49: 144-151.

Laissy, J.P., J.M. Serfaty, D. Messika-Zeitoun, A. Ribet, S. Chillon, P.G. Steg and I. Klein, 2009. Cardiac diffusion MRI of recent and chronic myocardial infarction: Preliminary results. J. Radiol., 90: 481-484.

Laissy, J.P., V. Gaxotte, L.E. Ironde, I. Klein and A. Ribet *et al*., 2013. Cardiac diffusion-weighted MR imaging in recent, subacute and chronic myocardial infarction: A pilot study. J. Magn. Reson. Imaging, 38: 1377-1387.

Le Bihan, D., 1995. Molecular diffusion, tissue microdynamics and microstructure. NMR Biomed., 8: 375-386.

Le Bihan, D., E. Breton, D. Lallemand, P. Grenier, E. Cabanis and M. Laval-Jeantet, 1986. MR imaging of intravoxel incoherent motions: Application to diffusion and perfusion in neurologic disorders. Radiology, 161: 401-407.

Lee, S.K., D.I. Kim, J. Kim, D.J. Kim, H.D. Kim, D.S. Kim and S. Mori, 2005. Diffusion-tensor MR imaging and fiber tractography: A new method of describing aberrant fiber connections in developmental CNS anomalies. Radiographics, 25: 53-65.

Lombaert, H., J.M. Peyrat, P. Croisille, S. Rapacchi and L. Fanton *et al*., 2012. Human atlas of the cardiac fiber architecture: Study on a healthy population. IEEE Trans. Med. Imag., 31: 1436-1447.

Malik, G.K., R. Trivedi, R.K. Gupta, K.M. Hasan and M. Hasan *et al*., 2006. Serial quantitative diffusion tensor MRI of the term neonates with hypoxic-ischemic encephalopathy (HIE). Neuropediatrics, 37: 337-343.

Manenti, G., M. Carlani, S. Mancino, V. Colangelo, M. di Roma, E. Squillaci and G. Simonetti, 2007. Diffusion tensor magnetic resonance imaging of prostate cancer. Invest. Radiol., 42: 412-419.

Mansfield, P., 1984. Real-time echo-planar imaging by NMR. Br. Med. Bull., 40: 187-190.

McGill, L.A., P.F. Ferreira, A.D. Scott, S. Nielles-Vallespin and A. Giannakidis *et al*., 2016. Relationship between cardiac diffusion tensor imaging parameters and anthropometrics in healthy volunteers. J. Cardiovasc. Magn. Reson., Vol. 18. 10.1186/s12968-015-0215-0

Moran, T.C., A.D. Kaye, A.H. Mai and L.R. Bok, 2013. Sedation, analgesia and local anesthesia: A review for general and interventional radiologists. RadioGraphics, 33: E47-E60.

Mori, S. and J. Zhang, 2006. Principles of diffusion tensor imaging and its applications to basic neuroscience research. Neuron, 51: 527-539.

Mori, S. and J.D. Tournier, 2013. Introduction to Diffusion Tensor Imaging: And Higher Order Models. Academic Press, USA., ISBN: 9780123984074, Pages: 140.

Mori, S., B.J. Crain, V.P. Chacko and V.P. Zijl, 1999. Three-dimensional tracking of axonal projections in the brain by magnetic resonance imaging. Ann. Neurol., 45: 265-269.

Moritani, T., S. Ekholm, P.L. Westesson and J. Zhong, 2005. Basics of Diffusion Measurements by MRI. In: Diffusion-Weighted MR Imaging of the Brain, Moritani, T., S. Ekholm and P.L. Westesson (Eds.). Springer, Germany, ISBN: 978-3-540-25359-4, pp: 1-5.

Moseley, M.E., Y. Cohen, J. Kucharczyk, J. Mintorovitch and H.S. Asgari *et al*., 1990. Diffusion-weighted MR imaging of anisotropic water diffusion in cat central nervous system. Radiology, 176: 439-445.

Nguyen, C., M. Lu, Z. Fan, X. Bi and P. Kellman *et al*., 2015. Contrast-free detection of myocardial fibrosis in hypertrophic cardiomyopathy patients with diffusion-weighted cardiovascular magnetic resonance. J. Cardiovasc. Magn. Reson., Vol. 17. 10.1186/s12968-015-0214-1

Nguyen, C., Z. Fan, B. Sharif, Y. He, R. Dharmakumar, D.S. Berman and D. Li, 2014. *In vivo* three-dimensional high resolution cardiac diffusion-weighted MRI: A motion compensated diffusion-prepared balanced steady-state free precession approach. Magn. Reson. Med., 72: 1257-1267.

Ni, H., V. Kavcic, T. Zhu, S. Ekholm and J. Zhong, 2006. Effects of number of diffusion gradient directions on derived diffusion tensor imaging indices in human brain. Am. J. Neuroradiol., 27: 1776-1781.

Nielles-Vallespin, S., C. Mekkaoui, P . Gatehouse, T.G. Reese and J. Keegan *et al*., 2013. *In vivo* diffusion tensor MRI of the human heart: Reproducibility of breath-hold and navigator-based approaches. Magn. Reson. Med., 70: 454-465.

Okayama, S., S. Uemura and Y. Saito, 2009. Detection of infarct-related myocardial edema using cardiac diffusion-weighted magnetic resonance imaging. Int. J. Cardiol., 133: e20-e21.

Okayama, S., S. Uemura, K. Onoue, Y. Takemoto and S. Somekawa *et al*., 2007. Infarct-related myocardial edema detected by diffusion-weighted imaging: Comparison with T2-weighted imaging. Circ., 116: II_772-II_772.

Ozmen, E., Y. Kayadibi, C. Samanci, N. Ustundag, G. Ozdemir, I. Adaletli and S. Kurugoglu, 2015. Primary pericardial synovial sarcoma in an adolescent patient: Magnetic resonance and diffusion-weighted imaging features. J. Pediatr. Hematol./Oncol., 37: e230-e233.

Polders, D.L., A. Leemans, J. Hendrikse, M.J. Donahue, P.R. Luijten and J.M. Hoogduin, 2011. Signal to noise ratio and uncertainty in diffusion tensor imaging at 1.5, 3.0 and 7.0 Tesla. J. Magn. Reson. Imaging, 33: 1456-1463.

Posse, S., C.A. Cuenod and D. Le Bihan, 1993. Human brain: Proton diffusion MR spectroscopy. Radiology, 188: 719-725.

Potet, J., A. Rahmouni, J. Mayer, A. Vignaud and P. Lim *et al*., 2013. Detection of myocardial edema with low-b-value diffusion-weighted echo-planar imaging sequence in patients with acute myocarditis. Radiol., 269: 362-369.

Rabi, I.I., J.R. Zacharias, S. Millman and P. Kusch, 1938. A new method of measuring nuclear magnetic moment. Phys. Rev., 53: 318-318.

Raja, A., J.R. Walker, M. Sud, J. Du and M. Zeglinski *et al*., 2011. Diagnosis of pericardial cysts using diffusion weighted magnetic resonance imaging: A case series. J. Med. Case Rep., Vol. 5. 10.1186/1752-1947-5-479

Reese, T.G., O. Heid, R.M. Weisskoff and V.J. Wedeen, 2003. Reduction of eddy-current-induced distortion in diffusion MRI using a twice-refocused spin echo. Magn. Reson. Med., 49: 177-182.

Reese, T.G., R.M. Weisskoff, R.N. Smith, B.R. Rosen, R.E. Dinsmore and V.J. Wedeen, 1995. Imaging myocardial fiber architecture *in vivo* with magnetic resonance. Magn. Reson. Med., 34: 786-791.

Rohmer, D. and G.T. Gullberg, 2006. A bloch-torrey equation for diffusion in a deforming media. Lawrence Berkeley National Laboratory. https://escholarship.org/uc/item/3zp3z6pw#page-2.

Romano, S., N. Boddaert, I. Desguerre, L. Hubert and R. Salomon *et al*., 2006. Molar tooth sign and superior vermian dysplasia: A radiological, clinical and genetic study. Neuropediatrics, 37: 42-45.

Santarelli, X., G. Garbin, M. Ukmar and R. Longo, 2010. Dependence of the fractional anisotropy in cervical spine from the number of diffusion gradients, repeated acquisition and voxel size. Magn. Reson. Imaging, 28: 70-76.

Scholz, T.D., S.R. Fleagle, T.L. Burns and D.J. Skorton, 1989. Nuclear magnetic resonance relaxometry of the normal heart: Relationship between collagen content and relaxation times of the four chambers. Magn. Reson. Imag., 7: 643-648.

Seo, Y., Z.J. Wang, M.C. Morriss and N.K. Rollins, 2012. Minimum SNR and acquisition for bias-free estimation of fractional anisotropy in diffusion tensor imaging-a comparison of two analytical techniques and field strengths. Magn. Reson. Imaging, 30: 1123-1133.

Soares, J., P. Marques, V. Alves and N. Sousa, 2013. A hitchhikers guide to diffusion tensor imaging. Front. Neurosci., 7: 31-31.

Sosnovik, D.E., R. Wang, G. Dai, T. Wang and E. Aikawa *et al*., 2009. Diffusion spectrum MRI tractography reveals the presence of a complex network of residual myofibers in infarcted myocardium. Circulat.: Cardiovasc. Imag., 2: 206-212.

Stanisz, G.J., E.E. Odrobina, J. Pun, M. Escaravage and S.J. Graham *et al*., 2005. T1, T2 relaxation and magnetization transfer in tissue at 3T. Magn. Reson. Med., 54: 507-512.

Stejskal, E.O. and J.E. Tanner, 1965. Spin diffusion measurements: Spin echoes in the presence of a time-dependent field gradient. J. Chem. Phys., 42: 288-292.

Stejskal, E.O., 1965. Use of spin echoes in a pulsed magnetic-field gradient to study anisotropic, restricted diffusion and flow. J. Chem. Phys., 43: 3597-3603.

Stoeck, C.T., C. von Deuster, M. Genet, D. Atkinson and S. Kozerke, 2016. Second-order motion-compensated spin echo diffusion tensor imaging of the human heart. Magn. Reson. Med., 75: 1669-1676.

Taylor, D.G. and M.C. Bushell, 1985. The spatial mapping of translational diffusion coefficients by the NMR imaging technique. Phys. Med. Biol., 30: 345-349.

Teraoka, K., H. Sakuma, M. Kawade, S. Kiuchi and Y. Suzuki *et al*., 2008. 300 diagnostic value of low b value diffusion weighted MRI in patients with acute myocardial infarction. J. Cardiovasc. Magn. Reson., Vol. 10. 10.1186/1532-429X-10-S1-A103.

Torrey, H.C., 1956. Bloch equations with diffusion terms. Phys. Rev., 104: 563-565.

Trivedi, R., R.K. Gupta, K.M. Hasan, P. Hou, K.N. Prasad and P.A. Narayana, 2006a. Diffusion tensor imaging in polymicrogyria: A report of three cases. Neuroradiology, 48: 422-427.

Trivedi, R., R.K. Gupta, A. Agarawal, K.M. Hasan and A. Gupta *et al*., 2006b. Assessment of white matter damage in subacute sclerosing panencephalitis using quantitative diffusion tensor MR imaging. Am. J. Neuroradiol., 27: 1712-1716.

Tuch, D.S., T.G. Reese, M.R. Wiegell, N. Makris, J.W. Belliveau and V.J. Wedeen, 2002. High angular resolution diffusion imaging reveals intravoxel white matter fiber heterogeneity. Magn. Reson. Med., 48: 577-582.

Turner, R., D. Le Bihan, J. Maier, R. Vavrek, L.K. Hedges and J. Pekar, 1990. Echo-planar imaging of intravoxel incoherent motion. Radiology, 177: 407-414.

Utsunomiya, H., S. Yamashita, K. Takano and M. Okazaki, 2006. Arrangement of fiber tracts forming Probst bundle in complete callosal agenesis: Report of two cases with an evaluation by diffusion tensor tractography. Acta Radiol., 47: 1063-1066.

Von Deuster, C., C.T. Stoeck, M. Genet, D. Atkinson and S. Kozerke, 2015. Spin echo versus stimulated echo diffusion tensor imaging of the *in vivo* human heart. Magn. Reson. Med. 10.1002/mrm.25998.

Wang, D., D. Ma, M.L. Wong and Y.X.J. Wang, 2015. Recent advances in surgical planning and navigation for tumor biopsy and resection. Quantit. Imag. Med. Surg., 5: 640-648.

Wu, L.M., B.H. Chen, Q.Y. Yao, Y.R. Ou and R. Wu *et al*., 2016. Quantitative diffusion-weighted magnetic resonance imaging in the assessment of myocardial fibrosis in hypertrophic cardiomyopathy compared with T1 mapping. Int. J. Cardiovasc. Imaging, 32: 1289-1297.

Wu, M.T., W.Y.I. Tseng, M.Y.M. Su, C.P. Liu and K.R. Chiou *et al*., 2006. Diffusion tensor magnetic resonance imaging mapping the fiber architecture remodeling in human myocardium after infarction correlation with viability and wall motion. Circ., 114: 1036-1045.

Yu, T., C. Zhang, A.L. Alexander and R.J. Davidson, 2013. Local tests for identifying anisotropic diffusion areas in human brain with DTI. Ann. Applied Stat., 7: 201-225.

Zhang, J., Y.M. Tehrani, L. Wang, N.M. Ishill, L.H. Schwartz and H. Hricak, 2008. Renal masses: Characterization with diffusion-weighted MR imaging-a preliminary experience. Radiology, 247: 458-464.